Molecules and Cells

CD38 Inhibition Protects Fructose-Induced Toxicity in Primary Hepatocytes

Soo-Jin Lee, Sung-E Choi, Seokho Park, Yoonjung Hwang, Youngho Son, and Yup Kang*

Department of Physiology, Ajou University School of Medicine, Suwon 16499, Korea
*Correspondence: kangy@ajou.ac.kr
https://doi.org/10.14348/molcells.2023.0045
www.molcells.org

A fructose-enriched diet is thought to contribute to hepatic injury in developing non-alcoholic steatohepatitis (NASH). However, the cellular mechanism of fructose-induced hepatic damage remains poorly understood. This study aimed to determine whether fructose induces cell death in primary hepatocytes, and if so, to establish the underlying cellular mechanisms. Our results revealed that treatment with high fructose concentrations for 48 h induced mitochondria-mediated apoptotic death in mouse primary hepatocytes (MPHs). Endoplasmic reticulum stress responses were involved in fructose-induced death as the levels of phosho-eIF2α, phospho-C-Jun-N-terminal kinase (JNK), and *C/EBP* homologous protein (CHOP) increased, and a chemical chaperone tauroursodeoxycholic acid (TUDCA) prevented cell death. The impaired oxidation metabolism of fatty acids was also possibly involved in the fructose-induced toxicity as treatment with an AMP-activated kinase (AMPK) activator and a PPAR-α agonist significantly protected against fructose-induced death, while carnitine palmitoyl transferase I inhibitor exacerbated the toxicity. However, uric acid-mediated toxicity was not involved in fructose-induced death as uric acid was not toxic to MPHs, and the inhibition of xanthine oxidase (a key enzyme in uric acid synthesis) did not affect cell death. On the other hand, treatment with inhibitors of the nicotinamide adenine dinucleotide (NAD)$^+$-consuming enzyme CD38 or CD38 gene knockdown significantly protected against fructose-induced toxicity in MPHs, and fructose treatment increased CD38 levels. These data suggest that CD38 upregulation plays a role in hepatic injury in the fructose-enriched diet-mediated NASH. Thus, CD38 inhibition may be a promising therapeutic strategy to prevent fructose-enriched diet-mediated NASH.

Keywords: apoptosis, CD38, endoplasmic reticulum stress, fructose, hepatocyte, non-alcoholic steatohepatitis

INTRODUCTION

Non-alcoholic fatty liver disease (NAFLD) is a medical condition characterized by the accumulation of fat in the liver, which is not caused by alcohol. It encompasses a disease spectrum ranging from simple fatty liver disease (steatosis) to non-alcoholic steatohepatitis (NASH) and cirrhosis (Berardo et al., 2020; Peng et al., 2020). NAFLD is associated with obesity and is considered a hepatic manifestation of insulin resistance (Gaggini et al., 2013). Intrahepatic fat accumulation generally results from the increased delivery of free fatty acids (FFAs) from adipose tissues to hepatocytes, enhanced *de novo* lipogenesis (DNL) and reduced fatty acid oxidation (FAO) in hepatocytes, and inadequate secretion of very low-density lipoproteins from hepatocytes (Nassir et al., 2015). Hepatic inflammation and injury are hallmarks of NASH and are key contributors to liver cirrhosis through the activation of collagen-producing stellate cells (Koyama and Brenner, 2017; Krenkel et al., 2018). Hepatic injury can initiate a sequence of events, from hepatic inflammation to hepatic fibrosis. Apoptotic bodies, damage-associated molecular patterns,

Received March 23, 2023; revised June 12, 2023; accepted June 14, 2023; published online July 27, 2023

eISSN: 0219-1032

and extracellular vesicles derived from damaged hepatocytes can activate quiescent hepatic Kupffer cells, which promote hepatic inflammation (Kanda et al., 2018). Meanwhile, hepatic inflammation can also contribute to hepatocyte demise (Brenner et al., 2013; Parthasarathy et al., 2020). Therefore, it is considered that there is a feedforward cycle of hepatocyte death and hepatic inflammation in NASH development. However, the cellular mechanisms of initial hepatic damage are not yet fully characterized in NASH.

Lipotoxicity caused by lipid derivative accumulation in hepatocytes is thought to play a role in initial hepatic damage in NAFLD (Marra and Svegliati-Baroni, 2018). Lipotoxicity is thought to occur when the cellular capacity to use, store and export FFAs in hepatocytes is overwhelmed by a massive FFA flux (Pardo et al., 2015; Rada et al., 2020). Although the exact cellular mechanism of lipotoxicity in hepatocytes has not been elucidated, the activation of stress signals through endoplasmic reticulum (ER) stress and/or oxidative stress and the subsequent activation of death signals have been reported to be involved in lipotoxicity-mediated cell death (Ly et al., 2020; Pardo et al., 2015). The breakage of ER homeostasis preferentially activates protein kinase RNA-like endoplasmic reticulum kinase (PERK), which phosphorylates eIF2α and promotes the transcription of *C/EBP* homologous protein (CHOP) and activating transcription factor 3 (ATF3). CHOP is known to trigger the mitochondria-mediated apoptotic pathway (Hu et al., 2019; Iurlaro and Munoz-Pinedo, 2016). Excessive ER stress can also stimulate IRE1α oligomerization, subsequently stimulating the activation of the apoptotic-signaling kinase-1 (ASK1) and C-Jun-N-terminal kinase (JNK). It is known that the excessive activation of ASK1 and JNK signals contributes to ER stress-induced cell death (Iurlaro and Munoz-Pinedo, 2016). Increased FAO upon FFA overload with an impairment of the mitochondrial electron transport complex and a reduction in the antioxidant system have been observed in NAFLD development (Begriche et al., 2013; Sunny et al., 2017). Thus, oxidative stress through reactive oxygen species (ROS) was also thought to play a role in hepatic damage in NAFLD (Spahis et al., 2017; Sunny et al., 2017).

Impaired energy metabolism in mitochondria has been suggested to play a role in NAFLD pathogenesis (Ramanathan et al., 2022). Cellular levels of nicotinamide adenine dinucleotide (NAD^+) display the energy state of cells (Covarrubias et al., 2021). Several reports have suggested that NAD^+ deficiency is a risk factor for NAFLD and thus, NAD^+ repletion has potential as a treatment for NAFLD (Gariani et al., 2016; Guarino and Dufour, 2019; Katsyuba et al., 2018; Xie et al., 2020). The cellular NAD^+ pool is maintained by a balance between the activity of NAD^+-synthesizing enzymes and NAD^+-consuming enzymes. NAD^+ can be synthesized through the *de novo* or salvage pathways (Supplementary Fig. S1) (Guarino and Dufour, 2019; Mouchiroud et al., 2013). The *de novo* pathway involves the synthesis of NAD^+ from tryptophan via kynurenine. NAD^+ can also be resynthesized from nicotinamide (NAM) in the salvage pathway. NAM is a byproduct of NAD^+ after the activation of NAD^+-utilizing enzymes such as sirtuins (SIRTs), poly (ADP-ribose) polymerases (PARPs), and CD38. NAM gets converted to NAD^+ via nicotinamide mononucleotide (NMN) using the enzymes nicotinamide phosphoribosyltransferase (NAMPT) and nicotinamide mononucleotide adenylyltransferase (NMNAT). NMN can also be produced from nicotinamide riboside (NR) through NR kinase. SIRTs are known to be NAD^+-dependent deacetylases and are considered as nutritional sensors (Houtkooper et al., 2012; Imai and Guarente, 2010). In most trials to increase SIRT activity through enhanced NAD^+ availability, NAFLD was ameliorated (Nassir and Ibdah, 2016; Zeng and Chen, 2022). The inhibition of α-amino-β-carboxymuconate-ε-semialdehyde decarboxylase (ACMSD), which boosts *de novo* NAD^+ synthesis, improved methionine-choline deficient diet-induced NAFLD in C57BL/6J mice and protected against fatty acid-induced apoptosis in primary mouse hepatocytes (Katsyuba et al., 2018). The protective effect of ACMSD inhibition was SIRT1-dependent. NMN and NR have been also used to boost cellular NAD^+ levels (Cantó et al., 2012; Yoshino et al., 2011). NR treatment has been shown to prevent high-fat/high-sucrose (HF/HS) diet-induced NAFLD through a SIRT1-dependnet functional improvement of mitochondria (Gariani et al., 2016). On the other hand, Pham et al. (2019) reported that NR treatment could reduce liver fibrosis without improvement of liver steatosis and inflammation in a HF/HS/high-cholesterol diet-induced mouse model of NAFLD. PARP-1 functions as a DNA repair enzyme, but excessive PARP activation depletes cellular NAD^+ and adenosine triphosphate (ATP) levels, leading to cell death (Andrabi et al., 2008; Martín-Guerrero et al., 2020). The development of HF/HS-induced NAFLD was shown to be associated with the induction of PARP expression and activity and a reduction in liver NAD^+ levels (Gariani et al., 2017). Treatment with a PARP inhibitor induced NAD^+ repletion and reversed HF/HS diet-induced NAFLD in a SIRT1-dependent manner (Gariani et al., 2017; Mukhopadhyay et al., 2017). CD38 is another NAD^+-consuming enzyme that produces ADP-ribose (ADPR) and NAM and is responsible for age-related NAD^+ decline (Camacho-Pereira et al., 2016). CD38 inhibition also protects against HF diet-induced NAFLD by activating the NAD^+/SIRT pathway (Xie et al., 2021).

Fructose is a monosaccharide in fruit and honey and is a major component of the sweeteners, such as sugar (a disaccharide of fructose and glucose) and corn syrup (a mixture of fructose and glucose monosaccharide). Epidemiological studies suggest that a fructose-enriched diet is a potent risk factor for NAFLD development and the transition from simple steatosis to NASH (Federico et al., 2021; Jensen et al., 2018). Fructose is almost exclusively metabolized in the liver, where it stimulates lipogenic programs through enhanced DNL and decreased FAO, contributing to the hepatic accumulation of lipids (Softic et al., 2016; 2019). Meanwhile, fructose metabolism is suggested to play a key role in inducing hepatic injury and inflammation as the knockout of fructokinase, which plays a role as the first enzyme of fructose metabolism, protects against HF/HS-induced steatohepatitis (Ishimoto et al., 2013; Roeb and Weiskichen, 2021). A fructose-enriched diet can induce ER stress and oxidative stress through elevated ROS and/or reactive nitrogen species levels in hepatocytes (Choi et al., 2017). However, the mechanism by which fructose metabolism is associated with the induction of ER and oxidative stress in hepatocytes remains unclear. The derange-

ment of purine metabolism is suggested to play a critical role in fructose-induced hepatic injury. The first reaction that produces fructose-1-phosphate from fructose can rapidly deplete the intrahepatic level of ATP and promote the production of adenosine monophosphate (AMP). Elevated AMP levels stimulate the production of uric acid as the final product of purine metabolism, which may be involved in hepatocyte death through oxidative stress and ER stress. Therefore, uric acid-mediated stress signals are considered important drivers of fructose-induced hepatotoxicity in fructose-enriched diet-induced NASH (Choi et al., 2014; Lanaspa et al., 2012; Zhang et al., 2017).

In view of the above, this study aimed to determine whether high fructose concentrations are toxic to primary hepatocytes and to determine the cellular mechanisms involved in the fructose-induced toxicity. Here, hepatocytes isolated from C57BL/6J mice were exposed to high fructose concentrations and fructose-induced cell death was then investigated using a cell death ELISA kit. The mode of cell death was elucidated by investigating the activation of caspase-3 and -9 and the release of mitochondrial cytochrome C into the cytosol. The levels of various signaling molecules were investigated via immunoblotting analysis. The effect of different stress signal inhibitors on fructose-induced toxicity were also investigated by measuring levels of cleaved caspase-3. The involvement of NAD^+ metabolism in fructose-induced toxicity was determined by investigating the effect of NAD^+-consuming enzyme inhibitors on fructose-induced death. The involvement of CD38 as an NAD^+ hydrolase was also determined by investigating the inhibitory effect of CD38 inhibitors or CD38 knockdown on fructose-induced toxicity. Finally, the upregulation of CD38 by fructose was also confirmed by analyzing the enzymatic activity of CD38.

MATERIALS AND METHODS

Reagents

The following chemicals were purchased from Sigma-Aldrich (USA): fructose, glucose, SP600125, SB203580, sodium salicylate, n-acetylcysteine (NAC), NG-monomethyl-L-arginine acetate (NMMA), metallothionein (MT), manganese (III) tetrakis (4-benzoic acid) porphyrin (MnTBAP), Go6976, Go698, myriocin, 5-tetradecyloxy-2-furoic acid, cerulenin, T0901317, troglitazone, rosiglitazone, etomoxir, bezafibrate, 5-aminoimidazole-4-carboxamide riboside, nicotinamide mononucleotide, NR, kynurenine, nicotinamide, GMX1772, FK866, sinefungin, L-methylnicotinamide, resveratrol, sirtinol, EX527, 3-aminobenzamide, 5-iodo-6-amino-1,2-benzopyrone, apigenin, quercetin, and allopurinol. Tauroursodeoxycholic acid (TUDCA) was obtained from Cayman Chemical (USA). H_2DCFDA (2′,7′-dichlorodihydrofluorescein diacetate) was purchased from Thermo Fisher Scientific (USA). C75 and 78c were purchased from MedChemExpress (USA). Antibodies against cleaved caspase-3, cleaved caspase-7, cleaved caspase-9, poly (ADP-ribose) polymerase, phospho-JNK (P-JNK), JNK (T-JNK), phospho-p38 (P-p38), p38 (T-p38), phospho-NFκB p65 (P-NFκB), p65 (T-NFκB), phospho-eIF2α (P-eIF2α), eIF2α (T-eIF2α), CHOP, ATF3, and SIRT3 were obtained from Cell Signaling Technology (USA). Antibodies against cytochrome C, NAMPT, nicotinamide mononucleotide adenyltransferase (NMNAT), SIRT1, CD38, and xanthine oxidase were purchased from Santa Cruz Biotechnology (USA). Anti-actin antibody was purchased from Bethyl Laboratories (USA).

Isolation of mouse primary hepatocytes (MPHs)

Primary hepatocytes were isolated from anesthetized, 8-week-old male C57BL/6J mice. Briefly, pre-perfusion buffer (140 mmol/L NaCl, 6 mmol/L KCl, 10 mmol/L HEPES [4-(2-hydroxyethyl)-1-piperazineethanesulfonic acid], and 0.2 mmol/L EGTA [ethylene glycol-bis (β-aminoethyl ether)-N,N,N′,N′-tetraacetic acid], pH 7.4) was injected through the hepatic artery of mice at a rate of 7 ml/min for 5 min and a collagenase-containing buffer (66.7 mmol/L NaCl, 6.7 mmol/L KCl, 5 mmol/L HEPES, 0.48 mmol/L $CaCl_2$, and 0.8 mg/ml type-IV collagenase, pH 7.4) was then perfused for 5 min. The liver sack was suspended in Medium 199 and ruptured with fine-tipped forceps. The cells were then released using a cell lifter and filtered twice through a 100-μm mesh. The dissociated hepatocytes were harvested via centrifugation (50 × *g*, 5 min), resuspended in Medium 199, and pelleted via centrifugation (200 × *g*, 7 min) using a 40% Percoll cushion. The pellets containing hepatocytes were resuspended in a complete growth medium (Medium 199 containing 10% fetal bovine serum) and the hepatocytes were then seeded in collagen-coated 12-well plates at a density of 2×10^5 cells/well. After a 4 h of incubation, the spent medium was replaced with fresh complete growth medium. Viable hepatocytes attached to the plate were used for further experiments.

Cell death assay

Cell death was determined by measuring the amount of histone-associated DNA fragments using a cell death detection ELISA kit (Roche Applied Science, Germany). Briefly, hepatocytes were lysed with a lysis buffer supplied by the kit and the lysates were then collected via centrifugation (200 × *g*, 10 min). The lysates were then pipetted onto an anti-streptavidin-coated microplate supplied with the kit. Anti-DNA monoclonal antibodies conjugated with peroxidase and anti-histone-biotin were then added to the plates and the plates were incubated at 25°C for 90 min. The wells were then rinsed three times with washing buffer (supplied by the kit). Color development was performed by adding a 2,2-azino-di-(3-ethylbenzthiazoline sulfonate) substrate solution, followed by shaking incubation at 250 rpm for 10-20 min. The amount of peroxidase retained in the nucleosome complex was determined by measuring the absorbance at 405 nm using a microplate reader. The amount of peroxidase retained in the nucleosome represents the degree of DNA fragmentation in the cells.

4′,6-diamidino-2-phenylindole (DAPI) staining

Nuclear condensation in primary hepatocytes was determined using DAPI staining. Briefly, primary hepatocytes were fixed with a 4% paraformaldehyde solution (Sigma-Aldrich) for 10 min and then washed twice with phosphate-buffered saline (PBS). The cells were permeabilized with 0.1% Triton X-100 for 15 min at room temperature, then incubated in a

DAPI solution (Thermo Fisher Scientific) for 10 min. The DAPI solution was removed, and the cells were observed using a Zeiss LSM 710 confocal microscope with an emission wavelength of 460 nm and an excitation wavelength of 350 nm.

Measurement of mitochondrial membrane potential

The reduction in mitochondrial membrane potential was assessed through the fluorescence shift of JC-1 aggregates in mitochondria from red to green using a JC-1 dye (Thermo Fisher Scientific). Briefly, primary hepatocytes were incubated with a 2 μM JC-1 staining solution (in Krebs-Ringer bicarbonate buffer) for 15 min in the dark, washed with PBS, resuspended in PBS and analyzed using a FACSAria III cell sorter (BD Biosciences, USA). The fluorescence intensity of the JC-1 aggregates and the JC-1 monomesr was measured at 590 nm (polyethylene filter) and at 529 nm (fluorescent isothiocyanate filter), respectively. The ratio of red to green was calculated using FACS Diva software (BD Biosciences).

Isolation of mitochondria

Mitochondria were isolated using a cell mitochondria isolation kit (Thermo Fisher Scientific) according to the manufacturer's instructions. Briefly, cells were suspended in the reagent A supplied by the kit and lysed using dounce homogenization after a short incubation on ice. The lysates were then mixed with the reagent C. The mitochondrial fraction was isolated by sequential centrifugation (initially at 700 × *g* for 10 min to obtain the supernatant containing mitochondria, then at 8,000 × *g* for 15 min to obtain the precipitates containing mitochondria). The proteins in the mitochondrial and cytosolic fractions were used to analyze cytochrome C release. Protein concentrations were the determined using Bradford assays (Thermo Fischer Scientific).

Immunoblotting

RIPA lysis buffer (Thermo Fisher Scientific) containing a protease inhibitor cocktail (Merck, Germany) was used to extract cellular proteins. Equivalent amounts of protein (20 μg) were suspended in sodium dodecyl sulfate (SDS) sample buffer (50 mM Tris-HCl, 2% SDS, 100 mM DL-dithiothreitol, and 10% glycerol, pH 6.8), separated via SDS-polyacrylamide gel electrophoresis (SDS-PAGE), then transferred to polyvinylidene difluoride (PVDF) membranes (Millipore, USA). The membranes were then blocked with 5% skimmed milk solution for 30 min. The target antigens were allowed to react with the appropriate primary antibodies, then with horseradish peroxidase-conjugated anti-mouse IgG or anti-rabbit IgG secondary antibodies. Immunoreactive bands were detected using an enhanced chemiluminescence system (Pierce, USA). Band intensities were determined via densitometric analysis using Image J software (NIH, USA).

ROS measurements

ROS levels were evaluated using the cell-permeant dye, H_2D-CFDA (Thermo Fisher Scientific). Trypsin-dissociated hepatocytes were immediately incubated in 20 μM H_2DCFDA-containing media for 30 min, then washed twice with PBS. The fluorescence intensity of the stained cells was analyzed using a FACSAria III flow cytometer (BD Biosciences). The excitation and emission wavelengths were 488 nm and 520 nm, respectively. Relative ROS levels were determined by measuring the MFIs (mean fluorescence intensities).

Transfection with siRNAs and CD38-expressing DNAs

SiRNAs were designed and synthesized by the Bioneer Corporation (South Korea). The sequences of siRNAs are listed in Supplementary Table S1. A CD38-expressing plasmid (pCMV-CD38) was obtained from Sino Biological (China). Plasmid DNA was prepared using a Qiagen plasmid midi kit. Primary hepatocytes were then transfected with siRNA oligonucleotides or plasmids using Lipofectamine 2000 (Thermo Fisher Scientific). Briefly, 2 × 10^5 primary hepatocytes were seeded into each well of a 12-well plate and incubated for 1 day. SiRNA or plasmid DNA was diluted in Opti-MEM without serum and Lipofectamine 2000 was also diluted in Opti-MEM. The diluted siRNA or plasmid DNA was combined with the diluted Lipofectamine 2000 (total volume = 100 μl), incubated for 20 min at room temperature, added to the hepatocytes, and incubated for 48 h. The cells were used to analyze target protein expression.

NAD^+/NADH ratio measurements

Total NAD (NADt: NAD^+ and NADH) and NADH levels were measured using an NAD^+/NADH quantification kit (Biovision). Briefly, hepatocytes were seeded in 6-well plates and cultured for 24 h. The cells were scraped, washed with PBS, and homogenized in the assay buffer supplied by the kit. Insoluble debris was removed via centrifugation (10,000 × *g*, 10 min), and the supernatants were then used to measure NADt or NADH levels. The supernatant was then mixed with the enzyme-containing cycling buffer supplied by the kit to convert residual NAD^+ to NADH. The level of NADH, including converted NADH, was measured to obtain the NADt level in the supernatant. To detect NADH levels in the supernatant, the NAD^+ in the supernatant was decomposed by heating the supernatant at 60°C for 30 min, and the remaining NADH was then detected. The amount of NADH was quantified by adding an NADH developer supplied from the kit, incubating at room temperature for 1 h, and measuring the absorbance at 450 nm. The quantity of NADt or NADH was determined based on the NADH standard curve generated. NAD^+ levels were obtained by subtracting NADH level from those of NADt. The NAD^+/NADH ratio in cells was obtained by dividing the NAD^+ level by the NADH level.

Reverse transcriptase-polymerase chain reaction (PCR)

Relative mRNA expression levels were measured using a Takara PrimeScript™ RT reagent kit and a TB Green® Premix Ex Taq™ II qPCR kit (Takara, Japan). Briefly, total RNA was extracted from hepatocytes using TRIzol reagent (Thermo Fisher Scientific) and cDNA was synthesized using PrimeScript RTase and random 9-mers. DNA amplification was performed using a TB Green® Premix Ex Taq™ II quantitative PCR kit under the following thermocycling conditions: initial denaturation at 95°C for 5 min, followed by 30 cycles of denaturation at 95°C for 30 s and annealing at 60°C for 30 s, and final extension at 72°C for 1 min. The following primer sequences were used: CD38 gene forward, 5′TGATCGCCTTGGTAGTAGGG3′; and

CD38 gene reverse, 5′CTTCGTGGTAGGCTCTCCAG3′. 36B4 gene forward, 5′CGACTCACAGAGCAGGC3′; 36B4 gene reverse, 5′CACCGAGGCAACAGTTGG-3′. The relative quantities of the amplified DNAs were analyzed using the software included with the Takara TP850 instrument (Takara).

CD38 activity measurements

The hydrolase/NADase activity of CD38 was measured using 1,N^6-ethenonicotinamide adenine dinucleotide (ε-NAD) fluorescence-based methods (de Oliveira et al., 2018). Primary hepatocytes were seeded in 6-well plates and incubated for 24 h. The cells were suspended in a sucrose buffer (0.25 mM sucrose, 40 mM Tris) and lysed via sonication on ice three times for 5 s. The supernatant containing CD38 was collected after centrifugation (10,000 × *g*, 10 min). Reactions were initiated by mixing the CD38-containing supernatant and ε-NAD substrate in reaction buffer (25 mM MES [2-(N-morpholino) ethanesulfonic acid], 150 mM NaCl, pH 6.5). Fluorescence signals were detected with a SpectraMax®iD3 multimode microplate reader (Molecular Devices, USA) for 30 min using excitation and emission wavelengths of 310 nm and 400 nm, respectively.

Statistical analysis

All experiments were repeated at least three times. Data are expressed as the mean ± SD. All data were analyzed using Prism 6.0 (GraphPad Software, USA). An unpaired Student's *t*-test was used to compare the two datasets. One-way or two-way ANOVA with the Bonferroni post hoc test was used when more than two datasets or groups were compared. Statistical significance was set at $P < 0.05$.

RESULTS

High fructose concentrations are cytotoxic to MPHs

Primary hepatocytes isolated from male C57BL/6J mice were treated with various fructose concentrations for 48 h to determine whether fructose was toxic to hepatocytes. Hepatocyte death was then determined by measuring the amount of histone-associated DNA fragments in the cytoplasm, which was found to be increased in a fructose concentration-dependent manner (Fig. 1A). This suggested that high fructose concentrations were cytotoxic to MPHs. Fructose-induced cytotoxicity was also time-dependent (Fig. 1B). Incubation for 48 h was sufficient to show distinct fructose toxicity. In conjunction with increased histone-associated DNA fragments, DAPI staining showed nuclear fragmentation in fructose-treated MPHs (Fig. 1C). In contrast, treatment with 20 mM glucose for 48 h did not induce cell death in MPHs (Supplementary Fig. S2A). This suggested that the toxic effect of monosaccharides on hepatocytes was specific to fructose. In addition, fructose-induced toxicity was specific to primary hepatocytes since treatment with 20 mM fructose for 48 h did not induce cell death in other hepatocyte cell lines, including HepG2, Hep3B, and Huh7 (Supplementary Fig. S2B). Mitochondrial membrane potential, cytochrome C release from the mitochondria to the cytoplasm, and caspase activation were then investigated to determine whether fructose-induced toxicity was related to mitochondria-mediated apoptotic cell death. Fructose treatment reduced mitochondrial membrane potential but increased the release of cytochrome C into the cytoplasm (Figs. 1D and 1E). Moreover, fructose increased the levels of cleaved caspases-9, -3, and -7, as well as those of cleaved PARP, a target molecule of caspase-3 (Fig. 1F). Together, these data suggest that a high fructose concentration was toxic to MPHs, which was mediated by the activation of the mitochondria-mediated apoptosis pathway.

Involvement of stress responses in fructose-induced toxicity

The levels of the P-JNK, P-p38, and P-NFκB were then measured in fructose-treated hepatocytes, and the protective effects of each signal inhibitor on fructose-induced caspase-3 activation were investigated to determine whether stress/inflammatory signals are involved in fructose-induced toxicity. The levels of P-JNK, P-p38, and P-NFκB significantly increased following fructose treatment (Fig. 2A). While sodium salicylate (an NFκB inhibitor) treatment did not affect fructose-induced caspase-3 activation, SP600125 and SB203580, which are inhibitors of JNK and p38, respectively, showed protective effects against fructose-induced toxicity (Fig. 2B). Since JNK and p38 are stress signals involved in the oxidative and ER stress response, the role of oxidative stress and ER stress in fructose-induced toxicity was investigated (Iurlaro and Munoz-Pinedo, 2016; Zhou et al., 2006). ROS levels were not significantly changed by fructose treatment and fructose-induced caspase-3 activation was unaffected by most antioxidant chemicals, including NAC, NMMA, MT, and MnTBAP (Figs. 2C and 2D). These data show that ROS and oxidative stress signals do not play a critical role in fructose-induced toxicity. Meanwhile, phosphorylated eIF2α and CHOP levels increased in fructose-treated MPHs and fructose-induced caspase-3 activation was significantly attenuated after treatment with the ER chaperone TUDCA (Figs. 2E and 2F). This suggests that ER stress responses are involved in fructose-induced toxicity in hepatocytes. The involvement of uric acid as an inducer of oxidative and ER stress was also investigated in fructose-induced toxicity. Treatment with allopurinol (a xanthine oxidase inhibitor) or the knockdown of xanthine oxidase did not affect fructose-induced toxicity (Supplementary Fig. S3). In addition, uric acid itself was not toxic to MPHs (Supplementary Fig. S3). This suggests that uric acid produced from fructose metabolism was not involved in fructose-induced toxicity in hepatocytes.

Involvement of lipid metabolism in fructose-induced toxicity

Fructose stimulates lipogenic programs through enhanced DNL and decreased FAO. Therefore, lipotoxicity caused by derangement of lipid metabolism may play a role in fructose-induced hepatocyte toxicity. The effects of several lipid metabolism modulators on fructose-induced toxicity were investigated to determine whether lipid metabolism is involved in fructose-induced toxicity. Protein kinase C (PKC) can be activated by diacylglycerol as a lipotoxic derivative; therefore, the effect of PKC inhibitors on fructose-induced toxicity was investigated. Treatment with Go6976 (a PKC α/β inhibitor), Go6983 (a pan-PKC inhibitor), or chelerythrine (a cell-permeable pKC inhibitor) did not affect fructose-induced

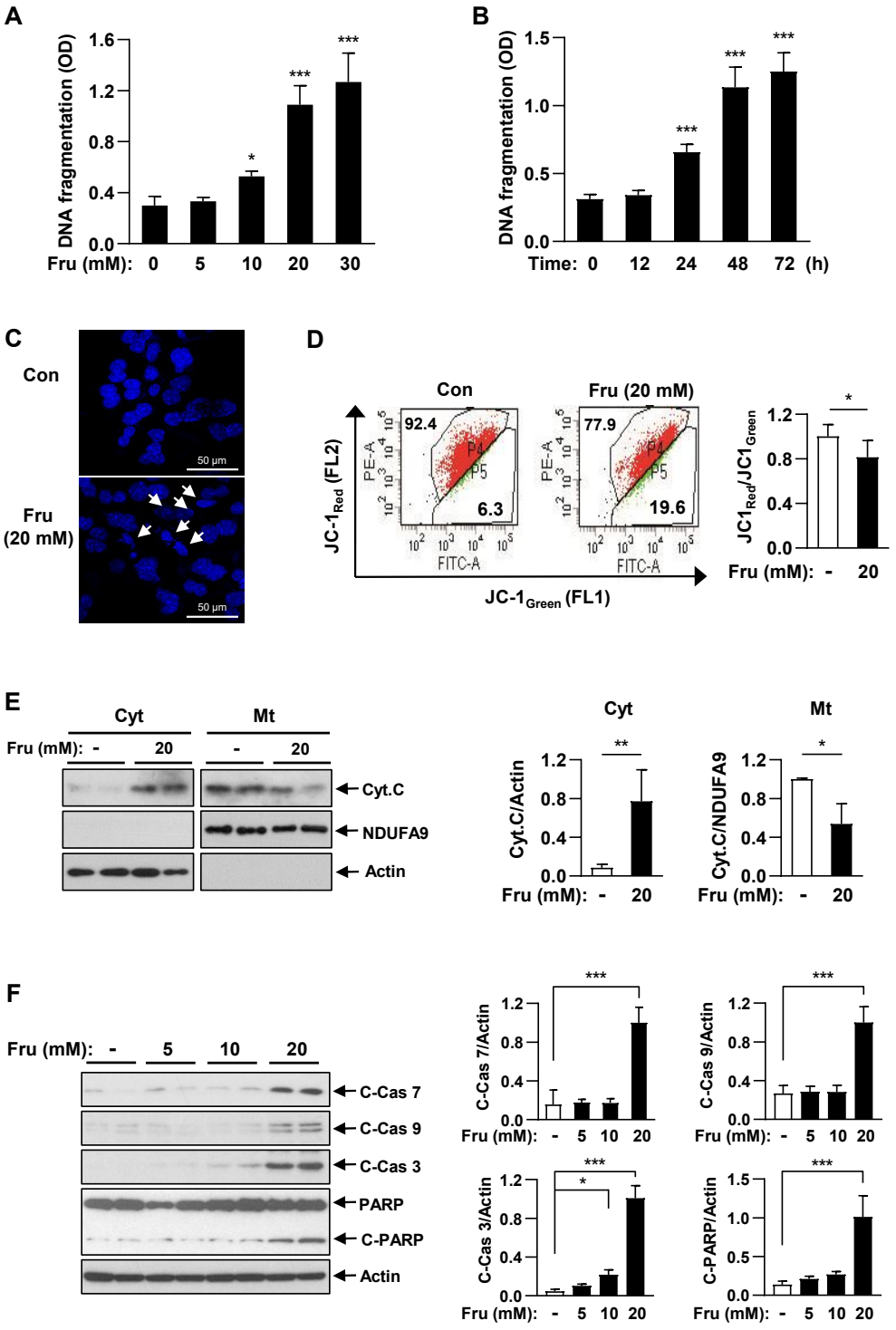

Fig. 1. Fructose induces cell death in mouse primary hepatocytes (MPHs). MPHs were isolated from 8-week-old male C57BL/6J mice and treated with different fructose (Fru) concentrations for 48 h or with 20 mM fructose for the indicated times. Cell death was determined using a cell death detection ELISA (A and B). Nuclear fragmentation was investigated via DAPI staining followed by fluorescence microscopy. White arrows indicate fragmented nuclei (C). Mitochondrial membrane potential change was determined by measuring the fluorescence shift after JC-1 staining (D). Cytochrome C (Cyt. C) release from the mitochondria (Mt) to cytosol (Cyt) was investigated through immunoblotting (E). The levels of cleaved caspase-7 (C-Cas 7), cleaved caspase-9 (C-Cas 9), cleaved caspase-3 (C-Cas 3), and cleaved poly (ADP-ribose) polymerase (C-PARP) in MPHs treated at different fructose concentrations were determined via immunoblotting (F). The data represent the mean ± SD. $*P < 0.05$, $**P < 0.01$, $***P < 0.001$ versus fructose-untreated MPHs. OD, optical density; Con, control.

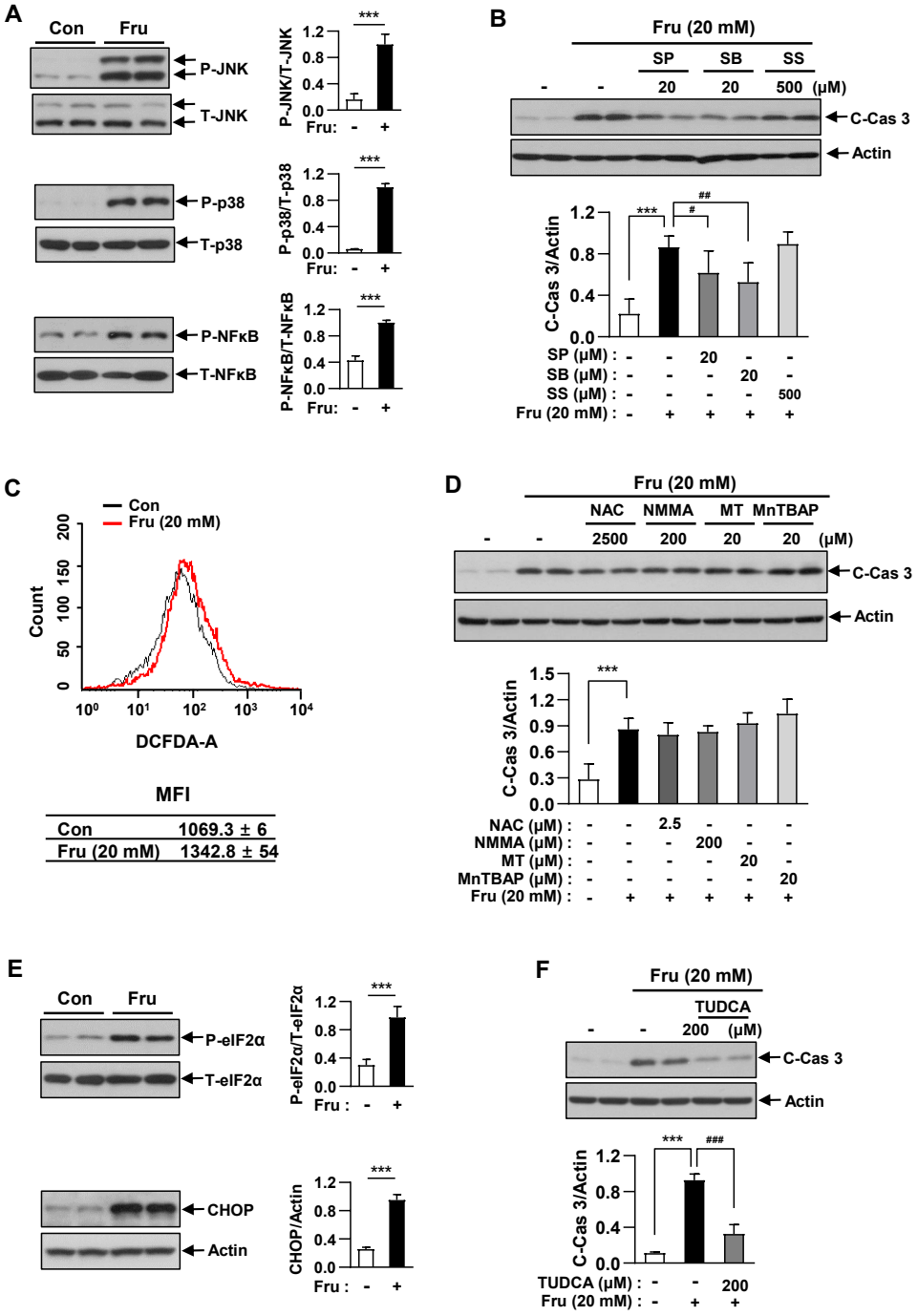

Fig. 2. Involvement of stress signals in fructose-induced cell death. Mouse primary hepatocytes (MPHs) were treated with 20 mM fructose (Fru) for 48 h. The levels of phospho-Jun-N-terminal kinase (P-JNK), phospho-p38 (P-p38), and phospho-nuclear factor kappa B (P-NFκB) were determined via immunoblotting analysis (A). The effect of stress signal inhibitors on fructose-induced cell death was investigated as the reduction of cleaved caspase-3 (C-Cas 3) levels in MPHs treated with 20 mM fructose in the presence of a JNK inhibitor (SP600125: SP), p38 inhibitor (SB203580: SB), or NFκB inhibitor (sodium salicylate: SS) (B). The levels of reactive oxygen species (ROS) were determined by measuring the mean fluorescence intensity (MFI) obtained through flow cytometry in dichlorofluorescin diacetate (DCFDA)-stained MPHs (C). The effect of antioxidants on fructose-induced cell death was determined by measuring the C-Cas 3 level in fructose-treated MPHs in the presence of various antioxidants (N-acetyl-L-cysteine [NAC], NG-monomethyl-L-arginine [NMMA], mito TEMPO [MT], and manganese tetrakis (4-benzoic acid) porphyrin [MnTBAP]) (D). The levels of P-eIF2α and *C/EBP* homologous protein (CHOP) were determined via immunoblotting analysis (E). The effect of endoplasmic reticulum chaperones on fructose-induced cell death was determined through the reduction in C-Cas 3 levels in fructose-treated MPHs in the presence of tauroursodeoxycholic acid (TUDCA) (F). The data represent the mean ± SD. $^{***}P < 0.001$ versus fructose-untreated MPHs. $^{\#}P < 0.05$, $^{\#\#}P < 0.01$, $^{\#\#\#}P < 0.001$ versus fructose-treated MPHs. Con, control.

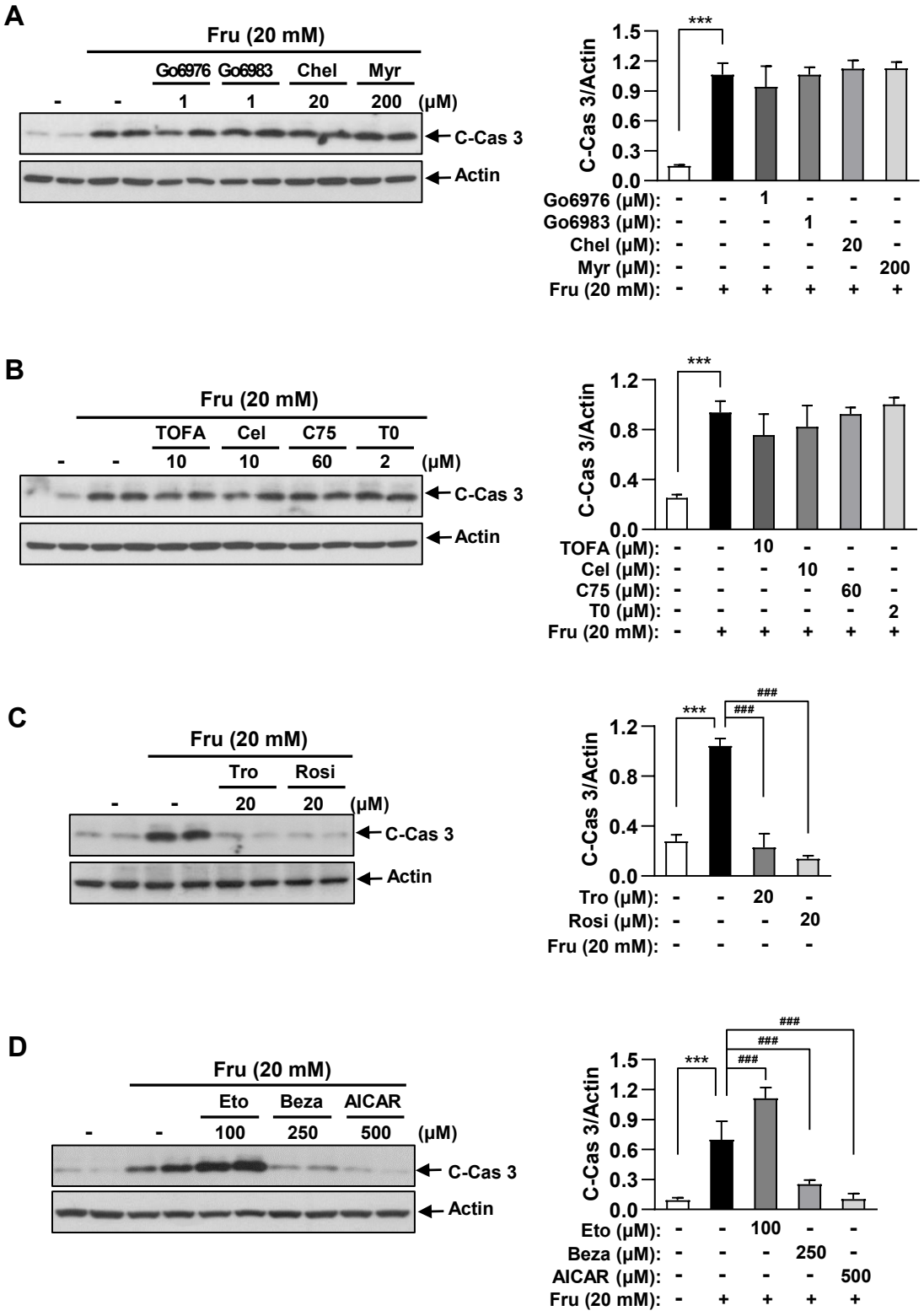

Fig. 3. Involvement of lipid metabolism in fructose-induced cell death. Mouse primary hepatocytes (MPHs) were treated with 20 mM fructose (Fru) for 48 h in the presence of lipid metabolism-related drugs (Go6976, Go6983, chelerythrine [Chel], myriocin [Myr], 5-(tetradecyloxy)-2-furoic acid [TOFA], cerulenin [Cel], C75, T0901317 [T0], troglitazone [Tro], rosiglitazone [Rosi], etomoxir [Eto], bezafibrate [Beza], and 5-aminoimidazole-4-carboxamide ribonucleotide [AICAR]). The protective effect of these inhibitors on fructose-induced cell death was determined via the reduction of cleaved caspase-3 (C-Cas 3) levels. The data represent the mean ± SD. $^{***}P < 0.001$ versus fructose-untreated MPHs. $^{###}P < 0.001$ versus fructose-treated MPHs.

toxicity (Fig. 3A). Myriocin, an inhibitor of serine palmitoyl transferase involved in ceramide synthesis, did not protect against fructose-induced toxicity (Fig. 3A). Moreover, 5-tetradecyloxy-2-furoic acid (an inhibitor of acetyl-CoA carboxylase [ACC]), cerulenin (an inhibitor of fatty acid synthase [FAS]), and C75 (an inhibitor of FAS) did not protect against fructose-induced toxicity (Fig. 3B). In addition, treatment with T0901317 (an agonist of nuclear receptor liver X receptor involved in lipid synthesis and cholesterol transport) did not affect fructose-induced toxicity in MPHs (Fig. 3B). However, troglitazone and rosiglitazone, which are agonists of peroxisome proliferator-activated receptor gamma (PPAR-γ) that plays a role in adipogenesis and insulin sensitivity, protected cells against fructose-induced toxicity (Fig. 3C). A PPAR-α agonist (bezafibrate) and AMPK activator (5-aminoimidazole-4-carboxamide riboside [AICAR]) significantly protected cells against fructose-induced toxicity. In contrast, etomoxir (a carnitine palmitoyl transferase I [CPT1] inhibitor) that inhibits FAO in mitochondria augmented fructose-induced toxicity in MPHs (Fig. 3D). These data indicate that the blockage of FAO metabolism may play a key role in fructose-induced toxicity.

Involvement of NAD^+ metabolism in fructose-induced toxicity

To determine whether changes in NAD^+ metabolism were involved in fructose-induced toxicity, NAD^+ levels were initially measured, and the effect of NAD^+ modulators on fructose-induced toxicity was then investigated by measuring cleaved caspase-3 levels. NAD^+ levels were not significantly changed by fructose treatment, but NADH levels slightly increased; thus, the ratio of NAD^+/NADH was significantly reduced (Fig. 4A, Supplementary Fig. S4). Supplementation with NMN or kynurenine as an NAD^+ precursor did not affect fructose-induced toxicity (Fig. 4B). In addition, supplementation with NR as an NAD^+ booster augmented fructose-induced toxicity (Fig. 4B). In contrast, NAM as a precursor for NAD^+ synthesis and an inhibitor of NAD^+-consuming enzymes significantly protected cells against fructose-induced toxicity (Fig. 4B). Interestingly, the inhibition of NAMPT as the enzyme catalyzing the first step of the NAD^+ synthesis salvage pathway protected cells against fructose-induced toxicity. Treatment with NAMPT inhibitors (GMX1772 and FK866) or NAMPT knockdown showed a protective effect against fructose-induced toxicity (Figs. 4C and 4D). In contrast, treatment with nicotinamide N-methyltransferase (NNMT) inhibitors (sinefugin and 1-methylnicotinamide) or NMMT knockdown did not affect fructose-induced toxicity (Figs. 4E and 4F). These data suggest that the protective effect of NAM on fructose-induced toxicity is due to its inhibitory role in NAD^+-consuming enzymes rather than NAD^+ supplementation as an NAD^+ precursor.

Involvement of CD38 activation in fructose-induced toxicity

The effect of activators or inhibitors of NAD^+-consuming enzymes on fructose-induced toxicity was also investigated to determine which NAD^+-consuming enzyme is involved in fructose-induced toxicity. Our results showed that treatment with resveratrol (an activator of SIRT1 and SIRT3), sirtinol (an inhibitor of SIRT1 and SIRT2), and EX527 (an inhibitor of SIRT1, SIRT2, and SIRT3) did not affect fructose-induced toxicity (Fig. 5A). In addition, the knockdown of SIRT1 and SIRT3 did not affect fructose-induced toxicity (Figs. 5B and 5C). PARP inhibitors (3-aminobenzamide and 5-iodo-6-amino-1,2-benzopyrone) did not protect against fructose-induced toxicity (Fig. 5D), as did PARP knockdown (Fig. 5E). In contrast, CD38 inhibitors (apigenin and quercetin) significantly protected cells against fructose-induced toxicity (Fig. 5F). In particular, a novel CD38 specific inhibitor (78c) showed a dose-dependent inhibitory effect on fructose-induced toxicity (Fig. 5G) and normalized the NAD^+/NADH ratio (Supplementary Fig. S5). CD38 overexpression augmented fructose-induced toxicity, whereas CD38 knockdown inhibited it (Figs. 5H and 5I). Fructose treatment significantly increased the expression and enzymatic activity of CD38 in MPHs (Figs. 5J-5L). Next, the levels of P-JNK, CHOP, and ATF3 were measured in fructose-treated hepatocytes in the presence of a CD38 inhibitor to confirm the involvement of CD38 in fructose-induced stress signal activation. Treatment with 78c significantly prevented the fructose-induced increase in the levels of P-JNK, CHOP, and ATF3 (Fig. 6A). Similarly, the knockdown of CD38 also reduced the fructose-induced increase in the levels of P-JNK, CHOP, and ATF3 (Fig. 6B). Meanwhile, CD38 overexpression further augmented the fructose-induced increase in the levels of P-JNK, CHOP, and ATF3 (Fig. 6C).

DISCUSSION

This study was conducted to elucidate the cellular mechanisms underlying fructose-induced toxicity in primary hepatocytes. High fructose concentrations induce mitochondria-mediated apoptotic death in MPHs. Uric acid and uric acid-mediated oxidative stress were unlikely to be involved in fructose-induced toxicity because uric acid alone was non-toxic to MPHs, and the inhibition of xanthine oxidase did not protect against fructose-induced cell death. In addition, oxidative stress was unlikely to be involved in toxicity because ROS levels did not increase and most antioxidants did not protect against fructose-induced death. Meanwhile, ER stress seems to be involved in fructose-induced cell death because ER stress signals are activated, and ER chaperone significantly prevents fructose-induced cell death. Lipid metabolism also seems to be involved in fructose-induced toxicity since treatment with lipid metabolism modulators such as AMPK activator, PPAR-γ agonist, and PPAR-α agonist strongly protected cells against fructose-induced cell death. In particular, inefficient FAO is thought to play a role in fructose-induced toxicity. Nicotinamide, an NAD^+-consuming enzyme inhibitor, showed a protective effect against fructose-induced toxicity. This suggests that NAD^+ metabolism is involved in fructose-induced toxicity. In particular, most trials to down-regulate the activity of CD38 as an NAD^+-consuming enzyme showed a strong protective effect against fructose-induced toxicity. Fructose treatment also enhanced CD38 activity in hepatocytes, suggesting that CD38 activation plays a role in fructose-induced toxicity in primary hepatocytes.

Exposing MPHs to high fructose concentrations induced mitochondria-mediated apoptotic death in a time- and dose-dependent manner. This indicates that long-term ex-

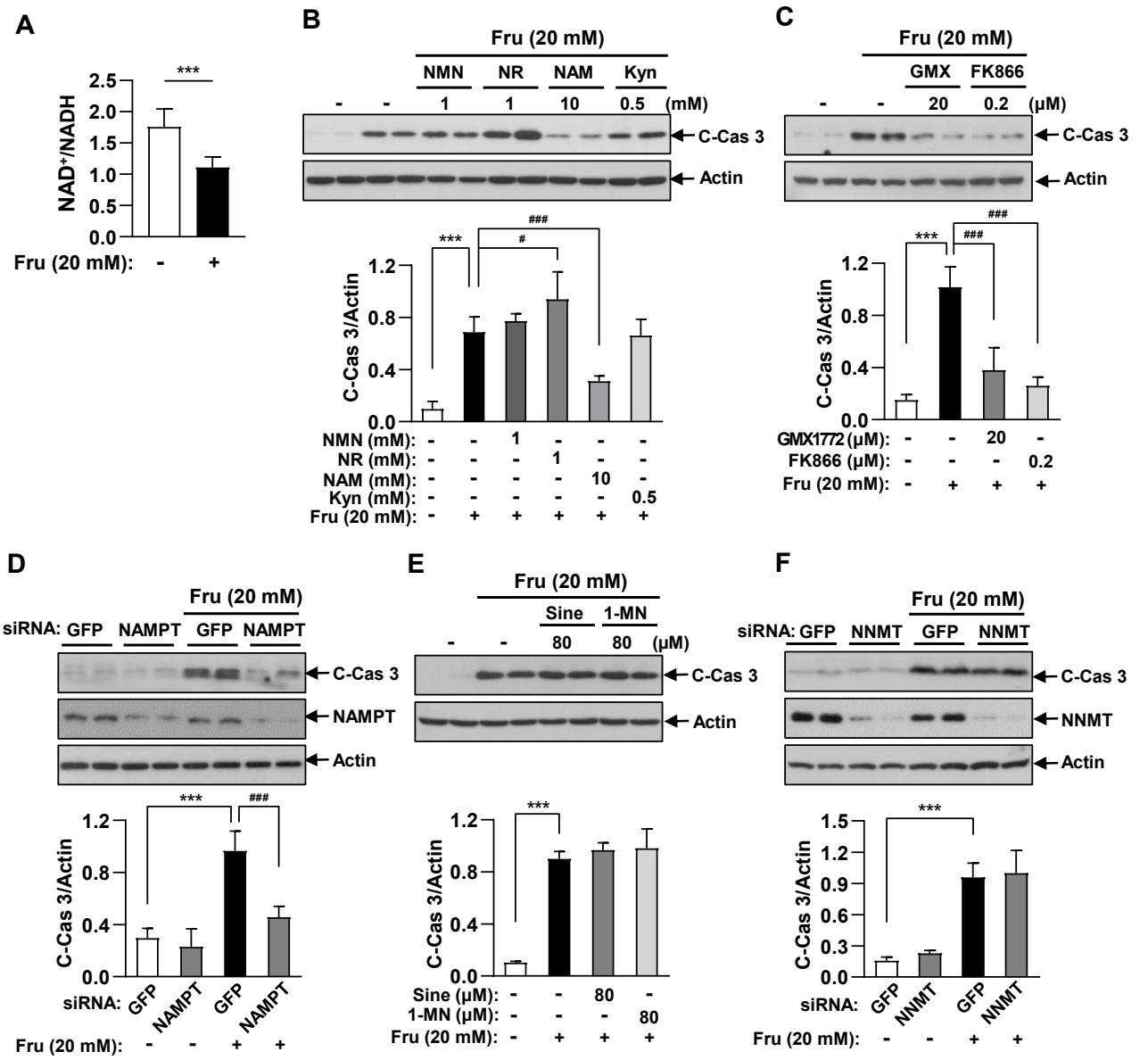

Fig. 4. Addition of nicotinamide (NAM) and inhibition of nicotinamide phosphorribosyltransferase (NAMPT) protects against fructose-induced cell death. Mouse primary hepatocytes (MPHs) were treated with 20 mM fructose (Fru) for 48 h and the NAD^+/NADH ratio in the cellular extract was determined by using an NAD^+/NADH quantification kit (A). MPHs were treated with 20 mM fructose for 48 h in the presence of nicotinamide mononucleotide (NMN), nicotinamide riboside (NR), NAM, and L-kynurenine (Kyn). The effect of these NAD^+ precursors on fructose-induced cell death was determined through the reduction of cleaved caspase-3 (C-Cas 3) levels (B). MPHs were treated with 20 mM fructose for 48 h in the presence of NAMPT inhibitors (GMX1772 [GMX], FK866) or NAMPT siRNA-transfected MPHs were treated with 20 mM fructose for 48 h. The effect of NAMPT downregulation on fructose-induced cell death was determined through the reduction of C-Cas 3 levels (C and D). MPHs were treated with 20 mM fructose for 48 h in the presence of nicotinamide *N*-methyltransferase (NNMT) inhibitors (sinefungin [Sine], 1-methylnicotinamide [1-MN]) or NNMT siRNA-transfected MPHs were treated with 20 mM fructose for 48 h. Cell death was analyzed by measuring C-Cas 3 levels following immunoblotting (E and F). The data represent the mean ± SD. $^{***}P < 0.001$ versus fructose-untreated MPHs. $^{\#}P < 0.05$, $^{\#\#\#}P < 0.001$ versus fructose-treated MPHs.

posure of hepatocytes to high fructose levels in the liver may contribute to hepatocyte cell death. Fructose-induced toxicity in hepatocytes was specific to fructose because glucose was not toxic to these cells and was also specific to primary cells since fructose treatment did not induce cell death in various hepatocyte cancer cell lines. The exact mechanism of fructose toxicity to primary hepatocytes was not clearly elucidated. However, fructose-specific metabolism in hepatocytes and cell type-specific signaling in primary cells may determine fructose-specific toxicity to primary hepatocytes (DeBerardinis

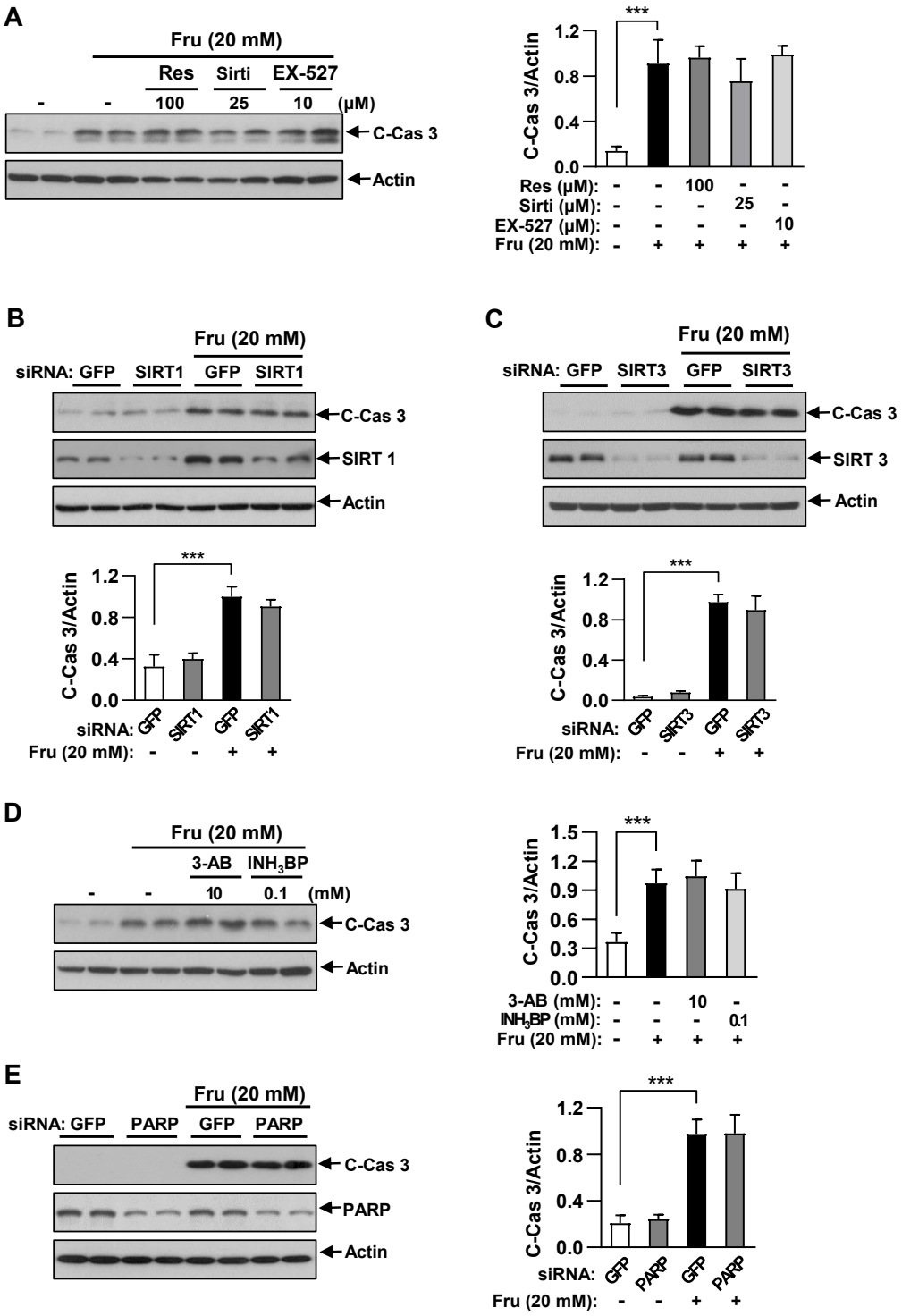

Fig. 5. CD38 inhibition protects against fructose-induced cell death. Mouse primary hepatocytes (MPHs) were treated with 20 mM fructose (Fru) for 48 h in the presence of sirtuin modulators (resveratrol [Res], sirtinol [Sirti], and EX-527), poly (ADP-ribose) polymerase (PARP) inhibitors (3-aminobenzamide [3-AB], 5-iodo-6-amino-1,2-benxopyrone [INH_3BP]), or CD38 inhibitors (apigenin [Apig], quercetin [Quer], and 78c) (A, D, F, and G). Fructose (20 mM) was added to SIRT1-knockdown (B), SIRT3-knockdown (C), PARP-knockdown, CD38-knockdown, or CD38-overexpressing MPHs for 48 h (B, C, E, H, and I). The effect of NAD^+-consuming enzyme modulators on fructose-induced cell death was determined through the reduction in cleaved caspase-3 (C-Cas 3) levels. The levels of CD38 mRNA and protein were analyzed via quantitative polymerase chain reaction and immunoblotting, respectively (J and K). The enzymatic activity of CD38 in fructose-treated MPHs was investigated using an *in vitro* fluorescence-based enzyme activity assay (L). The data represent the mean ± SD. $^{***}P < 0.001$ versus fructose-untreated MPHs. $^{\#}P < 0.05$, $^{\#\#\#}P < 0.001$ versus fructose-treated MPHs.

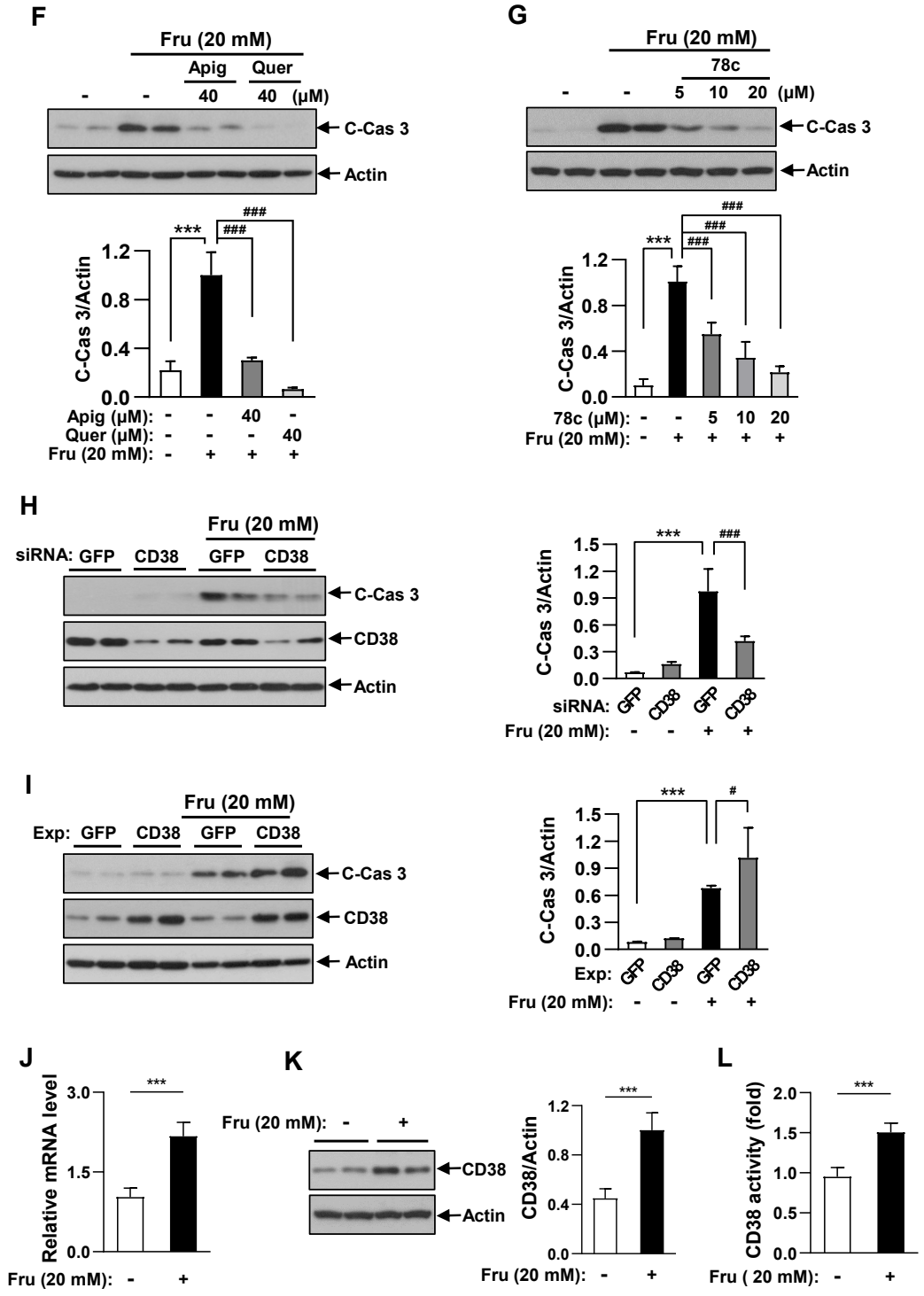

Fig. 5. Continued.

and Chandel, 2016; Geidl-Flueck and Gerber, 2017; Softic et al., 2017). The toxic effect observed after treatment with fructose concentrations above 10 mM did not seem to be represent a physiological concentration of fructose in blood. This is because the fructose concentration in the blood is reportedly lower than that of glucose because of its rapid metabolism in the liver (Sugimoto et al., 2010). However, the postprandial concentration of fructose in the portal vein could be increased to nearly 20 mM after fructose administration or ingestion through a sucrose-based diet (Hui et al., 2009), suggesting that the fructose levels used in this study may be at a physiologically probable concentration in the

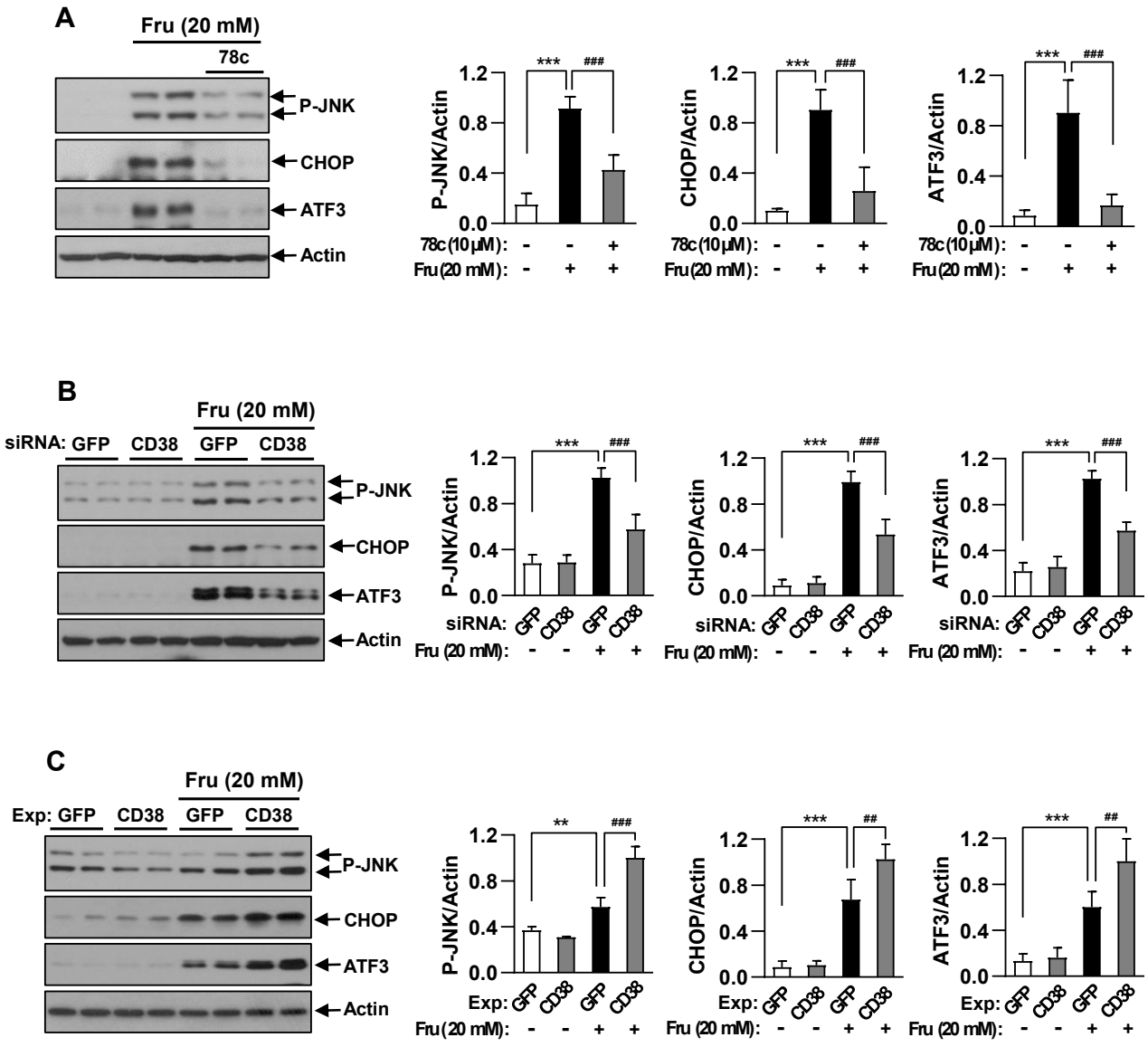

Fig. 6. Involvement of CD38 in fructose-induced stress signal activation. Mouse primary hepatocytes (MPHs) were treated with 20 mM fructose (Fru) for 48 h in the presence of 10 μM 78c (A). MPHs transfected with CD38 siRNAs (B) or CD38-expressing plasmids (C) were treated with 20 mM fructose for 48 h. The levels of endoplasmic reticulum stress-related molecules phosphor-Jun-N-terminal kinase (P-JNK), *C/EBP* homologous protein (CHOP), and activating transcription factor 3 (ATF3) were determined via immunoblotting analysis with anti-P-JNK, anti-CHOP, and anti-ATF3 antibodies, respectively. The data represent the mean ± SD. $^{**}P < 0.01$, $^{***}P < 0.001$ versus fructose-untreated MPHs. $^{\#\#}P < 0.01$, $^{\#\#\#}P < 0.001$ versus fructose-treated MPHs.

blood surrounding liver hepatocytes.

Uric acid accumulation in hepatocytes is thought to be a key mediator of fructose-induced hepatic damage in fructose-enriched diet-induced NASH. Uric acid can induce oxidative, mitochondrial, and ER stress responses in hepatocytes, which may activate the apoptotic pathway (Choi et al., 2014; Federico et al., 2021). However, our studies demonstrated that uric acid was not a mediator in fructose-induced death in hepatocytes because uric acid itself did not induce cell death in MPHs and moreover, the inhibition of xanthine oxidase, a key enzyme for uric acid synthesis from fructose, did not affect fructose-induced toxicity. On the other hand, fructose is a lipogenic substrate for DNL and a potent inducer of lipogenesis. Fructose can stimulate lipogenic gene expression through the transcriptional activation of *SREBP-1c* and *ChREBP*, resulting in lipid accumulation in hepatocytes (Berger and Moon, 2021; Softic et al., 2017). Therefore, lipotoxicity by lipid derivatives such as diacylglycerol, ceramides, and lysophosphatidic acid accumulated during the upregulation of the lipogenic pathway was suspected to be a key mediator for fructose-induced toxicity (Geng et al., 2021; Lipke et al., 2022). However, most inhibitors of PKCs activated by diacyl-

glycerol or an inhibitor of serine palmitoyl transferase, a key enzyme in ceramide synthesis, did not protect cells against fructose-induced toxicity. This suggests that lipid derivatives such as diacylglycerol and ceramides are not directly involved in fructose-induced toxicity. In addition, the augmentation of DNL and subsequent lipid accumulation may not be involved in fructose-induced toxicity because inhibitors of ACC and FAS did not affect fructose-induced toxicity. Meanwhile, agonists of nuclear receptors such as PPAR-γ and PPAR-α showed a strong protective effect against fructose-induced toxicity. Treatment with AMPK activator also prevented fructose-induced toxicity, while CPT1 inhibitor augmented this toxicity. These data suggest that impaired FAO metabolism may be involved in fructose-induced toxicity. Early studies reported that an increase in FAO metabolism by expanding the metabolic capacity of mitochondria prevents fatty acid-induced lipotoxicity, whereas impaired FAO is a key mediator of lipotoxicity (Haffar et al., 2015; Koves et al., 2008; Pimenta et al., 2008). It was also reported that a failure to manage excess fatty acids via impaired packaging into triacylglycerol is associated with hepatocyte lipototoxicty (Cazanave and Gores, 2010; Yamaguchi et al., 2007). Therefore, fructose-induced toxicity in MPHs is highly similar to fatty acid-induced lipotoxicity because an impairment in FAO metabolism is commonly involved in toxicity.

A decline in cellular NAD^+ levels and concurrent alterations in mitochondrial function are intrinsic to metabolic disorders, including NAFLD (Guarino and Dufour, 2019; Xie et al., 2020). In particular, hepatocyte-specific knockout of NAMPT aggravates dyslipidemia and liver damage in HF diet-fed mice, suggesting that low NAD^+ levels may be a critical mediator of NAFLD development (Wang et al., 2023). NMN and NR as NAD^+ boosters have been used as treatment to prevent NAFLD development (Cantó et al., 2012; Yoshino et al., 2011). Here, changes in NAD^+ levels following fructose treatment were investigated in MPHs to determine whether the changes in NAD^+ levels are involved in fructose-induced toxicity. We found that NAD^+ levels were not reduced following fructose treatment, while total NAD (including NADH) levels slightly increased. Notably, NAM exhibited a strong protective effect against fructose-induced toxicity. Because NAM is an NAD^+ byproduct resulting from the reaction of NAD^+-consuming enzymes and a recycling substrate for NMN synthesis, we investigated the protective effect of NMN on fructose-induced toxicity. Unexpectedly, NMN did not protect against fructose-induced toxicity. NR, as an NAD^+ booster via NMN, did not show a protective effect on fructose-induced toxicity. These data suggest that a decrease in NAD^+ level is not associated with fructose-induced hepatocyte toxicity and, thus, may not be involved in fructose-enriched diet-induced NAFLD. These results were somewhat contradictory to those reported in previous studies, wherein it was stated that an NAD^+ decline was involved in NAFLD pathogenesis. However, several studies also demonstrated that NAFLD pathogenesis was not necessarily dependent on decreased hepatic NAD^+ content, indicating that low NAD^+ level might not be the primary cause of NAFLD (Dall et al., 2018; Penke et al., 2015). On the other hand, NAMPT inhibition significantly protected against fructose-induced toxicity in our studies, suggesting that NAM accumulation through NAMPT inhibition may be involved in protective effect of NAMPT inhibition on fructose-induced toxicity. Collectively, we concluded that the protective role of NAM in the fructose-induced toxicity was caused by NAM itself rather than an NAD^+ booster. In fact, as NAM is known to inhibit various NAD^+-consuming enzymes (Bitterman et al., 2002; Klimova and Kristian, 2019; Salech et al., 2020), we suspected that the protective effect of NAM on fructose-induced toxicity was due to its inhibitory effect on the NAD^+-consuming enzymes. None of the chemical inhibitors of SIRTs or PARP showed any protective effects against fructose-induced toxicity. Moreover, the knockdown of the SIRTs or PARP did not show any protective effects. However, treatment with CD38 inhibitors or CD38 knockdown showed a significant protective effect against fructose-induced toxicity. These data indicate that CD38 inhibition plays a key role in NAM's protective effect on fructose-induced toxicity in MPHs.

We also investigated whether fructose upregulates the expression and activity of CD38 because a CD38 inhibitor or CD38 knockdown prevented fructose-induced toxicity. Fructose treatment increased the levels of CD38 mRNA and protein and the total activity of CD38 in MPHs. Because CD38 upregulation was observed in fructose-treated MPHs and ER stress was a key mediator in fructose-induced toxicity, we investigated whether CD38 upregulation is involved in fructose-induced ER stress. The inhibition or knockdown of CD38 prevented fructose-induced ER stress responses, whereas CD38 overexpression augmented fructose-induced ER stress. However, the mechanism by which fructose treatment increased the expression and activity of CD38 in hepatocytes was not clearly elucidated. Additionally, the mechanism through which CD38 activation induced ER stress and apoptosis signals remains unknown. It is suggested that CD38 overactivation may be involved in impaired FAO in the mitochondria; therefore, mitochondrial dysfunction may activate the apoptotic pathway in conjunction with the overactivation of ER stress signals. It is reported that CD38 inhibition protects against HF diet-induced NAFLD by activating the NAD^+/SIRT signaling pathway in hepatocytes (Xie et al., 2021). This report also suggests that fructose-induced toxicity overlaps with the hepatic lipotoxicity that occurs in HF diet-induced NAFLD.

In conclusion, long-term treatment with high fructose concentrations induces apoptotic cell death in primary hepatocytes. Fructose-induced toxicity is caused by the ER stress response, and ER stress was mediated by the upregulation of the NAD^+-consuming enzyme, CD38. Thus, CD38 inhibition could be a therapeutic strategy to prevent high fructose-enriched diet-induced NASH development.

Note: Supplementary information is available on the Molecules and Cells website (www.molcells.org).

ACKNOWLEDGMENTS

This work was supported by the National Research Foundation of Korea (NRF) grants (2018R1A6A3A11047049 and 2022R1A2C1091832) funded by the Korean government (MSIT).

AUTHOR CONTRIBUTIONS

S.J.L., S.E.C., S.P., Y.H., and Y.S. performed the experiments and contributed to the data acquisition. S.J.L. and Y.K. conceived and designed the study.

CONFLICT OF INTEREST

The authors have no potential conflicts of interest to disclose.

ORCID

Soo-Jin Lee https://orcid.org/0000-0002-9340-6290
Sung-E Choi https://orcid.org/0000-0002-1368-1912
Seokho Park https://orcid.org/0000-0002-0838-0429
Yoonjung Hwang https://orcid.org/0000-0003-1120-954X
Youngho Son https://orcid.org/0000-0002-6416-7024
Yup Kang https://orcid.org/0000-0002-9778-2015

REFERENCES

Andrabi, S.A., Dawson, T.M., and Dawson, V.L. (2008). Mitochondrial and nuclear cross talk in cell death: parthanatos. Ann. N. Y. Acad. Sci. *1147*, 233-241.

Berger, J.M. and Moon, Y.A. (2021). Increased hepatic lipogenesis elevates liver cholesterol content. Mol. Cells *44*, 116-125.

Begriche, K., Massart, J., Robin, M.A., Bonnet, F., and Fromenty, B. (2013). Mitochondrial adaptations and dysfunctions in nonalcoholic fatty liver disease. Hepatology *58*, 1497-1507.

Berardo, C., Di Pasqua, L.G., Cagna, M., Richelmi, P., Vairetti, M., and Ferrigno, A. (2020). Nonalcoholic fatty liver disease and non-alcoholic steatohepatitis: current issues and future perspectives in preclinical and clinical research. Int. J. Mol. Sci. *21*, 9646.

Bitterman, K.J., Anderson, R.M., Cohen, H.Y., Latorre-Esteves, M., and Sinclair, D.A. (2002). Inhibition of silencing and accelerated aging by nicotinamide, a putative negative regulator of yeast sir2 and human SIRT1. J. Biol. Chem. *277*, 45099-45107.

Brenner, C., Galluzzi, L., Kepp, O., and Kroemer, G. (2013). Decoding cell death signals in liver inflammation. J. Hepatol. *59*, 583-594.

Camacho-Pereira, J., Tarragó, M.G., Chini, C.C.S., Nin, V., Escande, C., Warner, G.M., Puranik, A S., Schoon, R.A., Reid, J.M., Galina, A., et al. (2016). CD38 dictates age-related NAD decline and mitochondrial dysfunction through an SIRT3-dependent mechanism. Cell Metab. *23*, 1127-1139.

Cantó, C., Houtkooper, R.H., Pirinen, E., Youn, D.Y., Oosterveer, M.H., Cen, Y., Fernandez-Marcos, P.J., Yamamoto, H., Andreux, P.A., Cettour-Rose, P., et al. (2012). The NAD(+) precursor nicotinamide riboside enhances oxidative metabolism and protects against high-fat diet-induced obesity. Cell Metab.*15*, 838-847.

Cazanave, S.C. and Gores, G.J. (2010). Mechanisms and clinical implications of hepatocyte lipoapoptosis. Clin. Lipidol. *5*, 71-85.

Choi, Y., Abdelmegeed, M.A., and Song, B.J. (2017). Diet high in fructose promotes liver steatosis and hepatocyte apoptosis in C57BL/6J female mice: role of disturbed lipid homeostasis and increased oxidative stress. Food Chem. Toxicol. *103*, 111-121.

Choi, Y.J., Shin, H.S., Choi, H.S., Park, J.W., Jo, I., Oh, E.S., Lee, K.Y., Lee, B.H., Johnson, R.J., and Kang, D. H. (2014). Uric acid induces fat accumulation via generation of endoplasmic reticulum stress and SREBP-1c activation in hepatocytes. Lab. Invest. *94*, 1114-1125.

Covarrubias, A.J., Perrone, R., Grozio, A., and Verdin, E. (2021). NAD^+ metabolism and its roles in cellular processes during ageing. Nat. Rev. Mol. Cell Biol. *22*, 119-141.

Dall, M., Penke, M., Sulek, K., Matz-Soja, M., Holst, B., Garten, A., Kiess, W., and Treebak, J.T. (2018). Hepatic NAD^+ levels and NAMPT abundance are unaffected during prolonged high-fat diet consumption in C57BL/6JBomTac mice. Mol. Cell Endocrinol. *473*, 245-256.

DeBerardinis, R.J. and Chandel, N.S. (2016). Fundamentals of cancer metabolism. Sci. Adv. *2*, e1600200.

de Oliveira, G.C., Kanamori, K.S., Auxiliadora-Martins, M., Chini, C.C.S., and Chini, E.N. (2018). Measuring CD38 hydrolase and cyclase activities: $1,N^6$-Ethenonicotinamide Adenine Dinucleotide (ε-NAD) and Nicotinamide Guanine Dinucleotide (NGD) fluorescence-based methods. Bio Protoc. *8*, e2938.

Federico, A., Rosato, V., Masarone, M., Torre, P., Dallio, M., Romeo, M., and Persico, M. (2021). The role of fructose in non-alcoholic steatohepatitis: old relationship and new insights. Nutrients *13*, 1314.

Gaggini, M., Morelli, M., Buzzigoli, E., DeFronzo, R.A., Bugianesi, E., and Gastaldelli, A. (2013). Non-alcoholic fatty liver disease (NAFLD) and its connection with insulin resistance, dyslipidemia, atherosclerosis and coronary heart disease. Nutrients *5*, 1544-1560.

Gariani, K., Menzies, K.J., Ryu, D., Wegner, C.J., Wang, X., Ropelle, E.R., Moullan, N., Zhang, H., Perino, A., Lemos, V., et al. (2016). Eliciting the mitochondrial unfolded protein response by nicotinamide adenine dinucleotide repletion reverses fatty liver disease in mice. Hepatology *63*, 1190-1204.

Gariani, K., Ryu, D., Menzies, K.J., Yi, H.S., Stein, S., Zhang, H., Perino, A., Lemos, V., Katsyuba, E., Jha, P., et al. (2017). Inhibiting poly ADP-ribosylation increases fatty acid oxidation and protects against fatty liver disease. J. Hepatol. *66*, 132-141.

Geidl-Flueck, B. and Gerber, P.A. (2017). Insights into the hexose liver metabolism-glucose versus fructose. Nutrients *9*, 1026.

Geng, Y., Faber, K.N., de Meijer, V.E., Blokzijl, H., and Moshage, H. (2021). How does hepatic lipid accumulation lead to lipotoxicity in non-alcoholic fatty liver disease? Hepatol. Int. *15*, 21-35.

Guarino, M. and Dufour, J.F. (2019). Nicotinamide and NAFLD: is there nothing new under the sun? Metabolites *9*, 180.

Haffar, T., Bérubé-Simard, F., and Bousette, N. (2015). Impaired fatty acid oxidation as a cause for lipotoxicity in cardiomyocytes. Biochem. Biophys. Res. Commun. *468*, 73-78.

Houtkooper, R.H., Pirinen, E., and Auwerx, J. (2012). Sirtuins as regulators of metabolism and healthspan. Nat. Rev. Mol. Cell Biol. *13*, 225-238.

Hu, H., Tian, M., Ding, C., and Yu, S. (2019). The C/EBP homologous protein (CHOP) transcription factor functions in endoplasmic reticulum stress-induced apoptosis and microbial infection. Front. Immunol. *9*, 3083.

Hui, H., Huang, D., McArthur, D., Nissen, N., Boros, L.G., and Heaney, A.P. (2009). Direct spectrophotometric determination of serum fructose in pancreatic cancer patients. Pancreas *38*, 706-712.

Imai, S. and Guarente, L. (2010). Ten years of NAD-dependent SIR2 family deacetylases: implications for metabolic diseases. Trends Pharmacol. Sci. *31*, 212-220.

Ishimoto, T., Lanaspa, M.A., Rivard, C.J., Roncal-Jimenez, C.A., Orlicky, D.J., Cicerchi, C., McMahan, R.H., Abdelmalek, M.F., Rosen, H.R., Jackman, M.R., et al. (2013). High-fat and high-sucrose (western) diet induces steatohepatitis that is dependent on fructokinase. Hepatology *58*, 1632-1643.

Iurlaro, R. and Muñoz-Pinedo, C. (2016). Cell death induced by endoplasmic reticulum stress. FEBS J. *283*, 2640-2652.

Jensen, T., Abdelmalek, M.F., Sullivan, S., Nadeau, K.J., Green, M., Roncal, C., Nakagawa, T., Kuwabara, M., Sato, Y., Kang, D.H., et al. (2018). Fructose and sugar: a major mediator of non-alcoholic fatty liver disease. J. Hepatol. *68*, 1063-1075.

Kanda, T., Matsuoka, S., Yamazaki, M., Shibata, T., Nirei, K., Takahashi, H., Kaneko, T., Fujisawa, M., Higuchi, T., Nakamura, H., et al. (2018). Apoptosis and non-alcoholic fatty liver diseases. World J. Gastroenterol. *24*, 2661-2672.

Katsyuba, E., Mottis, A., Zietak, M., De Franco, F., van der Velpen, V.,

Gariani, K., Ryu, D., Cialabrini, L., Matilainen, O., Liscio, P., et al. (2018). De novo NAD^+ synthesis enhances mitochondrial function and improves health. Nature *563*, 354-359.

Klimova, N. and Kristian, T. (2019). Multi-targeted effect of nicotinamide mononucleotide on brain bioenergetic metabolism. Neurochem. Res. *44*, 2280-2287.

Koves, T.R., Ussher, J.R., Noland, R.C., Slentz, D., Mosedale, M., Ilkayeva, O., Bain, J., Stevens, R., Dyck, J.R., Newgard, C. B., et al. (2008). Mitochondrial overload and incomplete fatty acid oxidation contribute to skeletal muscle insulin resistance. Cell Metab. *7*, 45-56.

Koyama, Y. and Brenner, D.A. (2017). Liver inflammation and fibrosis. J. Clin. Invest. *127*, 55-64.

Krenkel, O., Puengel, T., Govaere, O., Abdallah, A.T., Mossanen, J.C., Kohlhepp, M., Liepelt, A., Lefebvre, E., Luedde, T., Hellerbrand, C., et al. (2018). Therapeutic inhibition of inflammatory monocyte recruitment reduces steatohepatitis and liver fibrosis. Hepatology *67*, 1270-1283.

Lanaspa, M.A., Sanchez-Lozada, L.G., Choi, Y.J., Cicerchi, C., Kanbay, M., Roncal-Jimenez, C.A., Ishimoto, T., Li, N., Marek, G., Duranay, M., et al. (2012). Uric acid induces hepatic steatosis by generation of mitochondrial oxidative stress: potential role in fructose-dependent and -independent fatty liver. J. Biol. Chem. *287*, 40732-40744.

Lipke, K., Kubis-Kubiak, A., and Piwowar, A. (2022). Molecular Mechanism of lipotoxicity as an interesting aspect in the development of pathological states-current view of knowledge. Cells *11*, 844.

Ly, L.D., Ly, D.D., Nguyen, N.T., Kim, J.H., Yoo, H., Chung, J., Lee, M.S., Cha, S.K., and Park, K.S. (2020). Mitochondrial Ca2+ uptake relieves palmitate-induced cytosolic Ca2+ overload in MIN6 cells. Mol. Cells *43*, 66-75.

Marra, F. and Svegliati-Baroni, G. (2018). Lipotoxicity and the gut-liver axis in NASH pathogenesis. J. Hepatol. *68*, 280-295.

Martín-Guerrero, S.M., Casado, P., Hijazi, M., Rajeeve, V., Plaza-Díaz, J., Abadía-Molina, F., Navascués, J., Cuadros, M.A., Cutillas, P.R., and Martín-Oliva, D. (2020). PARP-1 activation after oxidative insult promotes energy stress-dependent phosphorylation of YAP1 and reduces cell viability. Biochem. J. *477*, 4491-4513.

Mouchiroud, L., Houtkooper, R.H., and Auwerx, J. (2013). NAD^+ metabolism: a therapeutic target for age-related metabolic disease. Crit. Rev. Biochem. Mol. Biol. *48*, 397-408.

Mukhopadhyay, P., Horváth, B., Rajesh, M., Varga, Z.V., Gariani, K., Ryu, D., Cao, Z., Holovac, E., Park, O., Zhou, Z., et al. (2017). PARP inhibition protects against alcoholic and non-alcoholic steatohepatitis. J. Hepatol. *66*, 589-600.

Nassir, F. and Ibdah, J.A. (2016). Sirtuins and nonalcoholic fatty liver disease. World J. Gastroenterol. *22*, 10084-10092.

Nassir, F., Rector, R.S., Hammoud, G.M., and Ibdah, J.A. (2015). Pathogenesis and prevention of hepatic steatosis. Gastroenterol. Hepatol. *11*, 167-175.

Pardo, V., González-Rodríguez, Á., Muntané, J., Kozma, S.C., and Valverde, Á.M. (2015). Role of hepatocyte S6K1 in palmitic acid-induced endoplasmic reticulum stress, lipotoxicity, insulin resistance and in oleic acid-induced protection. Food Chem. Toxicol. *80*, 298-309.

Parthasarathy, G., Revelo, X., and Malhi, H. (2020). Pathogenesis of nonalcoholic steatohepatitis: an overview. Hepatol. Commun. *4*, 478-492.

Peng, C., Stewart, A.G., Woodman, O.L., Ritchie, R.H., and Qin, C.X. (2020). Non-alcoholic steatohepatitis: a review of its mechanism, models and medical treatments. Front. Pharmacol. *11*, 603926.

Penke, M., Larsen, P.S., Schuster, S., Dall, M., Jensen, B.A., Gorski, T., Meusel, A., Richter, S., Vienberg, S.G., Treebak, J.T., et al. (2015). Hepatic NAD salvage pathway is enhanced in mice on a high-fat diet. Mol. Cell. Endocrinol. *412*, 65-72.

Pham, T.X., Bae, M., Kim, M.B., Lee, Y., Hu, S., Kang, H., Park, Y.K., and Lee, J.Y. (2019). Nicotinamide riboside, an NAD^+ precursor, attenuates the development of liver fibrosis in a diet-induced mouse model of liver fibrosis. Biochim. Biophys. Acta Mol. Basis Dis. *1865*, 2451-2463.

Pimenta, A.S., Gaidhu, M.P., Habib, S., So, M., Fediuc, S., Mirpourian, M., Musheev, M., Curi, R., and Ceddia, R.B. (2008). Prolonged exposure to palmitate impairs fatty acid oxidation despite activation of AMP-activated protein kinase in skeletal muscle cells. J. Cell. Physiol. *217*, 478-485.

Rada, P., González-Rodríguez, A., García-Monzón, C., and Valverde, Á.M. (2020). Understanding lipotoxicity in NAFLD pathogenesis: is CD36 a key driver? Cell Death Dis. *11*, 802.

Ramanathan, R., Ali, A.H., and Ibdah, J.A. (2022). Mitochondrial dysfunction plays central role in nonalcoholic fatty liver disease. Int. J. Mol. Sci. *23*, 7280.

Roeb, E. and Weiskirchen, R. (2021). Fructose and non-alcoholic steatohepatitis. Front. Pharmacol. *12*, 634344.

Salech, F., Ponce, D.P., Paula-Lima, A.C., SanMartin, C.D., and Behrens, M.I. (2020). Nicotinamide, a Poly [ADP-Ribose] polymerase 1 (PARP-1) inhibitor, as an adjunctive therapy for the treatment of Alzheimer's disease. Front. Aging Neurosci. *12*, 255.

Softic, S., Cohen, D.E., and Kahn, C.R. (2016). Role of dietary fructose and hepatic de novo lipogenesis in fatty liver disease. Dig. Dis. Sci. *61*, 1282-1293.

Softic, S., Meyer, J.G., Wang, G.X., Gupta, M.K., Batista, T.M., Lauritzen, H.P.M.M., Fujisaka, S., Serra, D., Herrero, L., Willoughby, J., et al. (2019). Dietary sugars alter hepatic fatty acid oxidation via transcriptional and post-translational modifications of mitochondrial proteins. Cell Metab. *30*, 735-753.e4.

Softic, S., Gupta, M.K., Wang, G.X., Fujisaka, S., O'Neill, B.T., Rao, T.N., Willoughby, J., Harbison, C., Fitzgerald, K., Ilkayeva, O., et al. (2017). Divergent effects of glucose and fructose on hepatic lipogenesis and insulin signaling. J. Clin. Invest. *127*, 4059-4074.

Spahis, S., Delvin, E., Borys, J.M., and Levy, E. (2017). Oxidative stress as a critical factor in nonalcoholic fatty liver disease pathogenesis. Antioxid. Redox Signal. *26*, 519-541.

Sugimoto, K., Hosotani, T., Kawasaki, T., Nakagawa, K., Hayashi, S., Nakano, Y., Inui, H., and Yamanouchi, T. (2010). Eucalyptus leaf extract suppresses the postprandial elevation of portal, cardiac and peripheral fructose concentrations after sucrose ingestion in rats. J. Clin. Biochem. Nutr. *46*, 205-211.

Sunny, N.E., Bril, F., and Cusi, K. (2017). Mitochondrial adaptation in nonalcoholic fatty liver disease: novel mechanisms and treatment strategies. Trends Endocrinol. Metab. *28*, 250-260.

Wang, D.X., Qing, S.L., Miao, Z.W., Luo, H.Y., Tian, J.S., Zhang, X.P., Wang, S.N., Zhang, T.G., and Miao, C.Y. (2023). Hepatic nampt deficiency aggravates dyslipidemia and fatty liver in high fat diet fed mice. Cells *12*, 568.

Xie, L., Wen, K., Li, Q., Huang, C.C., Zhao, J.L., Zhao, Q.H., Xiao, Y.F., Guan, X.H., Qian, Y.S., Gan, L., et al. (2021). CD38 deficiency protects mice from high fat diet-induced nonalcoholic fatty liver disease through activating NAD^+/Sirtuins signaling pathways-mediated inhibition of lipid accumulation and oxidative stress in hepatocytes. Int. J. Biol. Sci. *17*, 4305-4315.

Xie, N., Zhang, L., Gao, W., Huang, C., Huber, P.E., Zhou, X., Li, C., Shen, G., and Zou, B. (2020). NAD^+ metabolism: pathophysiologic mechanisms and therapeutic potential. Signal Transduct. Target. Ther. *5*, 227.

Yamaguchi, K., Yang, L., McCall, S., Huang, J., Yu, X.X., Pandey, S.K., Bhanot, S., Monia, B.P., Li, Y.X., and Diehl, A.M. (2007). Inhibiting triglyceride synthesis improves hepatic steatosis but exacerbates liver damage and fibrosis in obese mice with nonalcoholic steatohepatitis. Hepatology *45*, 1366-1374.

Yoshino, J., Mills, K.F., Yoon, M.J., and Imai, S. (2011). Nicotinamide mononucleotide, a key NAD(+) intermediate, treats the pathophysiology of diet- and age-induced diabetes in mice. Cell Metab. *14*, 528-536.

Zhang, D.M., Jiao, R.Q., and Kong, L.D. (2017). High dietary fructose: direct or indirect dangerous factors disturbing tissue and organ functions. Nutrients, *9*, 335.

Zhou, Y., Wang, Q., Mark Evers, B., and Chung, D.H. (2006). Oxidative stress-induced intestinal epithelial cell apoptosis is mediated by p38 MAPK. Biochem. Biophys. Res. Commun. *350*, 860-865.

Zeng, C. and Chen, M. (2022). Progress in nonalcoholic fatty liver disease: SIRT family regulates mitochondrial biogenesis. Biomolecules *12*, 1079.